Earth and Planetary Science Letters 416 (2015) 109–120

Contents lists available at ScienceDirect

Earth and Planetary Science Letters

www.elsevier.com/locate/epsl

Evidence for geochemical terranes on Mercury: Global mapping of major elements with MESSENGER's X-Ray Spectrometer

Shoshana Z. Weider [a,*], Larry R. Nittler [a], Richard D. Starr [b], Ellen J. Crapster-Pregont [c,d], Patrick N. Peplowski [e], Brett W. Denevi [e], James W. Head [f], Paul K. Byrne [a,g], Steven A. Hauck II [h], Denton S. Ebel [c,d], Sean C. Solomon [a,d]

[a] Department of Terrestrial Magnetism, Carnegie Institution of Washington, Washington, DC 20015, USA
[b] Physics Department, The Catholic University of America, Washington, DC 20064, USA
[c] Department of Earth and Planetary Sciences, American Museum of Natural History, New York, NY 10024, USA
[d] Lamont-Doherty Earth Observatory, Columbia University, Palisades, NY 10964, USA
[e] The Johns Hopkins University Applied Physics Laboratory, Laurel, MD 20723, USA
[f] Department of Earth, Environmental and Planetary Sciences, Brown University, Providence, RI 02912, USA
[g] Lunar and Planetary Institute, Universities Space Research Association, Houston, TX 77058, USA
[h] Department of Earth, Environmental, and Planetary Sciences, Case Western Reserve University, Cleveland, OH 44106, USA

ARTICLE INFO

Article history:
Received 29 September 2014
Received in revised form 5 January 2015
Accepted 21 January 2015
Editor: C. Sotin

Keywords:
Mercury
MESSENGER
X-ray fluorescence
spectroscopy
geochemistry

ABSTRACT

We have mapped the major-element composition of Mercury's surface from orbital MESSENGER X-Ray Spectrometer measurements. These maps constitute the first global-scale survey of the surface composition of a Solar System body conducted with the technique of planetary X-ray fluorescence. Full maps of Mg and Al, together with partial maps of S, Ca, and Fe, each relative to Si, reveal highly variable compositions (e.g., Mg/Si and Al/Si range over 0.1–0.8 and 0.1–0.4, respectively). The geochemical variations that we observe are consistent with those inferred from other MESSENGER geochemical remote sensing datasets, but they do not correlate well with units mapped previously from spectral reflectance or morphology. Location-dependent, rather than temporally evolving, partial melt sources were likely the major influence on the compositions of the magmas that produced different geochemical terranes. A large ($>5 \times 10^6$ km^2) region with the highest Mg/Si, Ca/Si, and S/Si ratios, as well as relatively thin crust, may be the site of an ancient and heavily degraded impact basin. The distinctive geochemical signature of this region could be the consequence of high-degree partial melting of a reservoir in a vertically heterogeneous mantle that was sampled primarily as a result of the impact event.

1. Introduction

Since the MErcury Surface, Space ENvironment, GEochemistry, and Ranging (MESSENGER) spacecraft (Solomon et al., 2001) was inserted into orbit around Mercury on 18 March 2011, its suite of instruments has been used to make measurements of the planet's surface composition. Mercury's ancient surface consists mostly of volcanic deposits that were likely produced by partial melting of the planet's mantle. The major-element composition of these rocks therefore provides important information on the behavior of the evolving mantle during Mercury's early history. The Mg and Al contents of surface materials are particularly good indicators of early differentiation and temporal evolution of partial melting processes at depth. Previous studies of MESSENGER datasets have shown that Mercury's surface is Mg- and S-rich, but Al-, Ca-, and Fe-poor compared with typical terrestrial and lunar crustal materials (e.g., Nittler et al., 2011; Evans et al., 2012), and that the planet has abundant levels of moderately volatile elements such as K (Peplowski et al., 2011, 2012) and Na (Peplowski et al., 2014). Considerable compositional heterogeneities across Mercury's surface have also been documented (Peplowski et al., 2012, 2014, 2015; Weider et al., 2012, 2014). The measured compositions indicate that Mercury's surface rocks are most similar to magnesian basalts (Stockstill-Cahill et al., 2012) and Fe-poor basaltic komatiites (Charlier et al., 2013).

Here we present global maps of the Mg/Si and Al/Si abundance ratios across Mercury's surface from data acquired by MESSENGER's X-Ray Spectrometer (XRS). These are the first global geochemical maps of Mercury, and indeed the first maps of global extent for any planetary body acquired via X-ray fluorescence (XRF).

* Corresponding author.
E-mail address: sweider@carnegiescience.edu (S.Z. Weider).

http://dx.doi.org/10.1016/j.epsl.2015.01.023
0012-821X/

Together with partial maps of S/Si, Ca/Si, and Fe/Si (Weider et al., 2014), these datasets provide a basis for investigating variations in major-element abundances across the surface of Mercury and their implications for the early history of the planet and its mantle evolution.

2. MESSENGER's X-Ray Spectrometer

The MESSENGER XRS consists of three planet-facing gas-proportional counter (GPC) detectors and a Sun-pointing Si-PIN detector within the Solar Assembly for X-rays (SAX) (Schlemm et al., 2007). All four detectors have an energy range of ~1–10 keV, but the energy resolution of the GPCs is insufficient to separate the fluorescent K_α lines of Mg, Al, and Si (at 1.25, 1.49, and 1.74 keV, respectively). A "balanced filter" approach (Starr et al., 2000) was therefore employed, in which thin foils of Mg and Al placed in front of two GPCs provide selective absorption at different energies and allow the fluorescent signals from these elements to be deconvolved (Adler et al., 1972; Trombka et al., 2000). The detector resolution at higher energies is sufficient to separate the characteristic fluorescence lines for elements at higher atomic number (Z) (i.e., S, Ca, Ti, and Fe).

XRS data integration periods vary with MESSENGER's location in its eccentric orbit. Integration times are shortest (to a minimum of 40 s) close to periapsis, which occurs over Mercury's high northern latitudes, and longest (up to 450 s) when the spacecraft is far from the planet. Collimators on the GPC detectors produce a hexagonal 12° field of view (FOV), which corresponds to a measurement "footprint" on the surface that varies in size from <100 km to >3000 km in effective diameter (Schlemm et al., 2007; Weider et al., 2012).

The X-ray spectra obtained by the GPC detectors can contain signals from a number of sources, which include: (i) background counts that arise from interactions between galactic cosmic rays or solar energetic particles and the detectors, (ii) characteristic fluorescent X-rays from the planet, (iii) solar X-rays scattered from the planet's surface, and (iv) episodic interactions between energetic electrons quasi-trapped in the planet's magnetosphere and the GPC detectors (e.g., Ho et al., 2012; Starr et al., 2012).

3. XRS data and analysis procedures

XRS measures characteristic XRF, induced by incident solar X-rays, from the top <100 μm of Mercury's surface. The XRS measurements are therefore sensitive to the highly variable solar X-ray flux (e.g., Bouwer, 1983). Characteristic XRF data can be obtained during two different phases of solar activity (see Fig. 1). During typical "quiet Sun" periods (i.e., when solar coronal plasma temperatures are less than ~8 MK), only XRF signals with energy less than ~2 keV (e.g., Mg, Al, and Si K_α lines) can be detected. During solar flare conditions, in contrast, heavier elements can be excited and produce measurable XRF. We generated element-ratio maps using a methodology (Weider et al., 2014) that combines XRF analyses with variable spatial resolution; see Section 5.

3.1. Flare data analysis

Previously published XRS results were based entirely on data obtained during solar flares. The flare analysis procedure we employed for this study follows Nittler et al. (2011) and Weider et al. (2012, 2014). Our forward modeling technique, based on the fundamental-parameters approach (e.g., Clark and Trombka, 1997; Nittler et al., 2001), is used to derive elemental abundances for Mercury's surface by fitting both the measured incident solar spectra and the planetary XRF spectra. The maps we present are derived from analyses of 731 individual measurements made during 457 solar flares (Table S1).

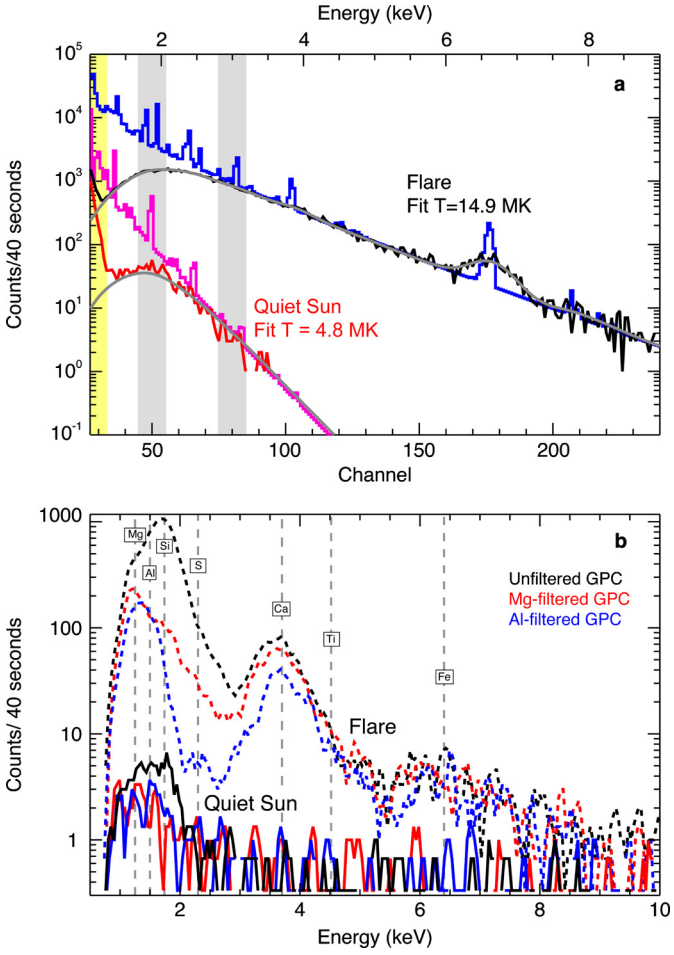

Fig. 1. Example MESSENGER XRS spectra (40 s integrations) from a solar flare (26 October 2013, 09:36 UTC) and a quiet-Sun period (18 October 2013, 01:21 UTC). (**a**) SAX solar spectra under flare (black) and quiet-Sun (red) conditions, and (**b**) the corresponding planetary XRF spectra from each GPC detector. Fits to the observed spectra in (**a**) are shown in grey, and the equivalent high-resolution solar flare spectra are shown in blue (flare) and pink (quiet Sun), along with the best-fit flare temperature (T). The yellow band indicates the spectral region dominated by electronic background. Grey bands show the channel ranges used to estimate the solar flare temperature for the quiet-Sun analysis (Section 3.2.3). Backgrounds have not been subtracted from the flare (dashed lines) and quiet-Sun (solid lines) spectra in (**b**). During flares, fluorescence from elements up to Fe is observed; during typical quiet-Sun periods fluorescence from only Mg, Al, and Si is detected and the overall signal level is much lower.

3.2. Quiet-Sun data analysis

3.2.1. Matrix inversion

It is more difficult to fit XRS spectra obtained during quiet-Sun conditions than during flare periods, for two reasons. First, the absence of fluorescence from high-Z elements removes several constraints on the spectral fitting parameters. Second, the large number ($>10^5$) of quiet-Sun spectra obtained during the MESSENGER mission makes the individual least-squares fitting approach (employed for the flare spectra) impractical. We thus developed a matrix-inversion approach to analyze the XRS quiet-Sun data. A similar methodology was used for analysis of Apollo 15 and 16 lunar XRF data (e.g., Yin et al., 1993).

For this approach, we assumed that the summed count rates for the GPC spectral channels (25–55), which cover the energy range 1.0–2.2 keV, are the result of the detector backgrounds plus the Mg, Al, and Si K_α XRF lines convolved with the relevant detector response at each energy: